1

2 **Potential for early forecast of Moroccan wheat yields based on climatic drivers**

3

4 **J. Lehmann[1], M. Kretschmer[2], B. Schauberger[1], and F. Wechsung[1]**

5 [1]Potsdam Institute for Climate Impact Research (PIK), Member of the Leibniz Association,
6 Potsdam, Germany

7 [2]University of Reading, Reading, United Kingdom

8

9 Corresponding author: Jascha Lehmann (jlehmann@pik-potsdam.de)

10

11 **Key Points:**

12 • Moroccan wheat yield anomalies are hindcasted four months before harvest based on
13   climate precursors.

14 • Precursors are extracted from gridded fields of climate variables using physically guided
15   causal discovery algorithms.

16 • The detected causal interactions are physically meaningful and consistent with
17   documented teleconnections in the climate system.

18   **Abstract**

19   Wheat production plays an important role in Morocco with the country typically producing more
20   than half of Northwest African grain production. Current wheat forecast systems use weather and
21   vegetation data during the crop growing phase, thus limiting the earliest possible release date to
22   early spring. However, Morocco's wheat production is mostly rainfed and thus strongly tied to
23   fluctuations in rainfall, which in turn depend on slowly evolving climate dynamics. This offers a
24   source of predictability at longer timescales. Using physically-guided causal discovery
25   algorithms we extract climate precursors for wheat yield variability from gridded fields of
26   geopotential height and sea surface temperatures which show potential for accurate yield
27   forecasts already in December. The detected interactions are physically meaningful and
28   consistent with documented ocean-atmosphere feedbacks. Reliable yield forecasts at such long
29   lead times could provide farmers and policy-makers with necessary information for early action
30   and strategic adaptation measurements to support food security.
31

32   **Plain Language Summary**

33   The per capita consumption of cereals in Morocco is one of the highest in the world placing a
34   significant role to wheat production in the framework of national food security. Early wheat
35   forecasts are crucial to increase the resilience of the agricultural sector to climate risks. So far,
36   operational forecast systems provide first yield estimates in March-April and hence around one
37   month before harvest starts in May. These systems use weather and vegetation data during the
38   crop growing phase thus limiting the earliest possible release date to this very time period. Here,
39   we present a different approach based on causal interactions in the climate system to provide
40   accurate forecasts of year-to-year wheat yield changes already in December. We make use of the
41   fact that wheat production is mostly rainfed and thus strongly coupled to prevailing rain
42   conditions which, in turn, are influenced by slowly evolving circulation patterns and sea surface
43   temperatures in the Atlantic and Pacific Ocean. These links between far-away regions, also
44   known as teleconnections, can last for several months and thus provide predictability at seasonal
45   timescales relevant for strategic adaptation decisions, e.g. regarding crop import planning or the
46   choice and intensity of agronomic practices.
47

48 **1 Introduction**

49 Agriculture is of particular strategic importance in Morocco. Most of the arable land is devoted
50 to cereals with wheat accounting for the majority of total cereal production and thus playing a
51 key factor for national food security. However, most of the arable land is located in arid or semi-
52 arid regions which are characterized by long dry periods and high year-to-year rainfall variations
53 (Born et al., 2008). Since very little of the arable land is irrigated, this leaves Morocco's wheat
54 production heavily dependent on large fluctuations in rainfall intensities (Berdai et al., 2011).
55 Reliable seasonal forecasts could help in reducing the vulnerability of the Moroccan agriculture
56 to weather risks by enabling timely in-season adaptation. Since the Moroccan climate is
57 projected to become drier and hotter with ongoing global warming, such forecasts will likely
58 become even more important in the future (Born et al., 2008; Filahi et al., 2017).
59
60 Operational yield forecasting systems provide estimates at lead times of a few days up to three
61 months before harvest in May-June. Provisional forecasts are released every year by the Crop
62 Growth Monitoring System – Morocco (CGMC-MAROC) in April and then constantly revised
63 over the course of the season. CGMS-MAROC uses a physical crop growth model combined
64 with statistical models (Bernardi, 2016; Bregaglio et al., 2014). Based on empirical regression
65 models using weather and vegetation data Balaghi et al. (2008) accurately forecast grain yields
66 as early as of March. Yet, both approaches use the Normalized Difference Vegetation Index
67 (NDVI) during mid-season of the growing phase which limits the earliest possible release date to
68 early spring.
69
70 Longer lead times may be achieved through utilization of remote climatic drivers which
71 influence rainfall variability over Morocco and thus wheat production. Total annual wheat yields
72 are significantly correlated to accumulated rainfall during the rainy season lasting from
73 September to May (De Wit et al., 2013). Intra-seasonal rainfall variability in turn is influenced
74 by large-scale climate dynamics including atmospheric circulation patterns and sea surface
75 temperatures over the Pacific and Atlantic Ocean which may persist over months allowing for
76 skillful forecasts at extended lead times (Knippertz et al., 2003; Rodríguez-Fonseca et al., 2006).
77 The most prominent mode of large-scale variability in the Atlantic, the North Atlantic Oscillation
78 (NAO), has been shown to directly influence the early stage of Moroccan wheat growth in
79 December by shaping the storm tracks which bring moist air from the Atlantic Ocean to the land
80 (Jarlan et al., 2014). Moreover, indirect influences on Moroccan rainfall may occur via
81 atmospheric teleconnections; wave trains, for instance, can emerge from sea surface temperature
82 forcing and may lead to temperature and rainfall changes in far-away regions downstream of the
83 wave (Schlueter et al., 2019; Shaman & Tziperman, 2011).
84
85 Tapping into this potential source of forecasting rainfall and thus Moroccan wheat yields, we
86 here apply a physically motivated approach based on causal discovery algorithms (Runge et al.,
87 2019) to find causal climate precursors for interannual wheat yield variability at least four

88 months before harvest. Previous studies have successfully applied the methodology of causal
89 precursors to forecast extreme stratospheric polar vortex states relevant for mid-latitude winter
90 weather (Kretschmer et al., 2017) and the Indian summer monsoon intensity (Di Capua et al.,
91 2019).
92
93 **2 Data**

94 Moroccan wheat yield (MWY) data. Nationally aggregated annual wheat yield data for the time
95 period 1979-2017 is taken from the website of the Food and Agriculture Organization (FAO)
96 (FAOSTAT, 2017) with wheat yields given in hectograms per hectare (hg/ha). Annual anomalies
97 are calculated based on the difference to the yield in the previous year (first differences) thereby
98 removing possible linear trends.
99 Climate data. Precursors are derived from two climate variables: sea surface temperature (SST)
100 and geopotential height at 500 hPa (Z500), with the latter being a commonly used level to
101 describe high and low pressure systems in the mid troposphere. We selected these climate
102 variables because they were shown to be linked to Moroccan winter climate and/or wheat yields
103 (e.g. Jarlan et al., 2014; Knippertz et al., 2003; Tuel & Eltahir, 2018). Both climate variables are
104 taken from the ERA5 reanalysis product provided on a 1° x 1° longitude-latitude grid covering
105 the time period 1979-2017 at monthly time resolution (Hersbach et al., 2019). Similarly, as for
106 the MWY time series, monthly climate anomalies are calculated at each grid cell by calculating
107 the difference to the same month of the previous year. Due to the first differences approach for
108 anomaly calculation and the wheat growing season lasting from November to June, the analysis
109 is limited to the years 1981-2017.
110
111 **3 Building the statistical forecast model – a three step approach**

112 Building the forecast model consists of three steps: (1) defining potential precursors from
113 gridded climate variables by hierarchical clustering of correlation maps, (2) selecting causal
114 precursors from potential precursors using causal discovery algorithms and (3) applying
115 multiple-linear regressions on observed yield anomalies using causal precursor time series.

116 **Step 1: Define potential precursors**
117 Potential precursors are defined as confined regions of a climate variable whose changes precede
118 changes in the target variable, i.e. nationally aggregated MWY anomalies. In a first step,
119 pairwise correlation analyses are conducted between MWY anomalies and lagged time series of
120 monthly Z500 and SST anomalies at each grid cell of the gridded globe between 90°N and 20°S
121 to include possible teleconnections from the northern hemisphere and the tropics. Thereby,
122 statistical significance at the grid cell level is defined at the 2% threshold (two-tailed p-value <
123 0.02). Using two climate variables (Z500 and SST) and four time lags (September to December)
124 thus leads to eight correlation maps from which potential precursors are extracted. Potential
125 precursors are defined by grouping significantly correlated grid cells of the same correlation sign
126 using Density-Based Spatial Clustering of Applications with Noise (DBSCAN, Ester et al., 1996;

127   Schubert et al., 2017). In DBSCAN a radius of 300 km is chosen to define neighboring grid cells
128   which is found to produce regions of reasonable sizes and spatial separation.

129   **Step 2: Select causal precursors from potential precursors**
130   So far potential precursor regions have been identified which are correlated with the target
131   variable MWY. These lagged correlations, however, do not necessarily imply causation. Non-
132   causal, spurious correlations can emerge from indirect links, common drivers or autocorrelation
133   effects. To remove such spuriously correlated precursors we apply a multivariate causal
134   discovery algorithm (Runge et al., 2019). The algorithm uses partial correlations to iteratively
135   check whether the link between a given potential precursor and the target variable can be
136   explained by any combination of the remaining potential precursors. If this is the case, i.e. if the
137   given potential precursor is conditionally independent from the target variable, then this potential
138   precursor is removed. Otherwise, it is considered as a causal precursor. A detailed step-by-step
139   description of this causal selection step can be found in Kretschmer et al. (2016). Despite the
140   thorough selection process the definition of causality given here, like any causal interpretation,
141   rests on several underlying assumptions (J. Runge, 2018). In this sense, causal precursors as
142   defined in this study should be understood as climatic indices which exhibit a significant, time-
143   lagged linear dependence with MWY anomalies that cannot be explained by any other identified
144   potential precursor or combination of those.
145   The combination of step 1 and step 2 of the method part was first introduced by Kretschmer et al.
146   (2017) as the response-guided causal precursor detection. Here, we apply the same method albeit
147   with the modification of clustering significantly correlated grid cells in step 1 in contrast to
148   merging only directly neighboring grid cells. This has shown to improve the robustness of
149   detecting potential precursor regions.
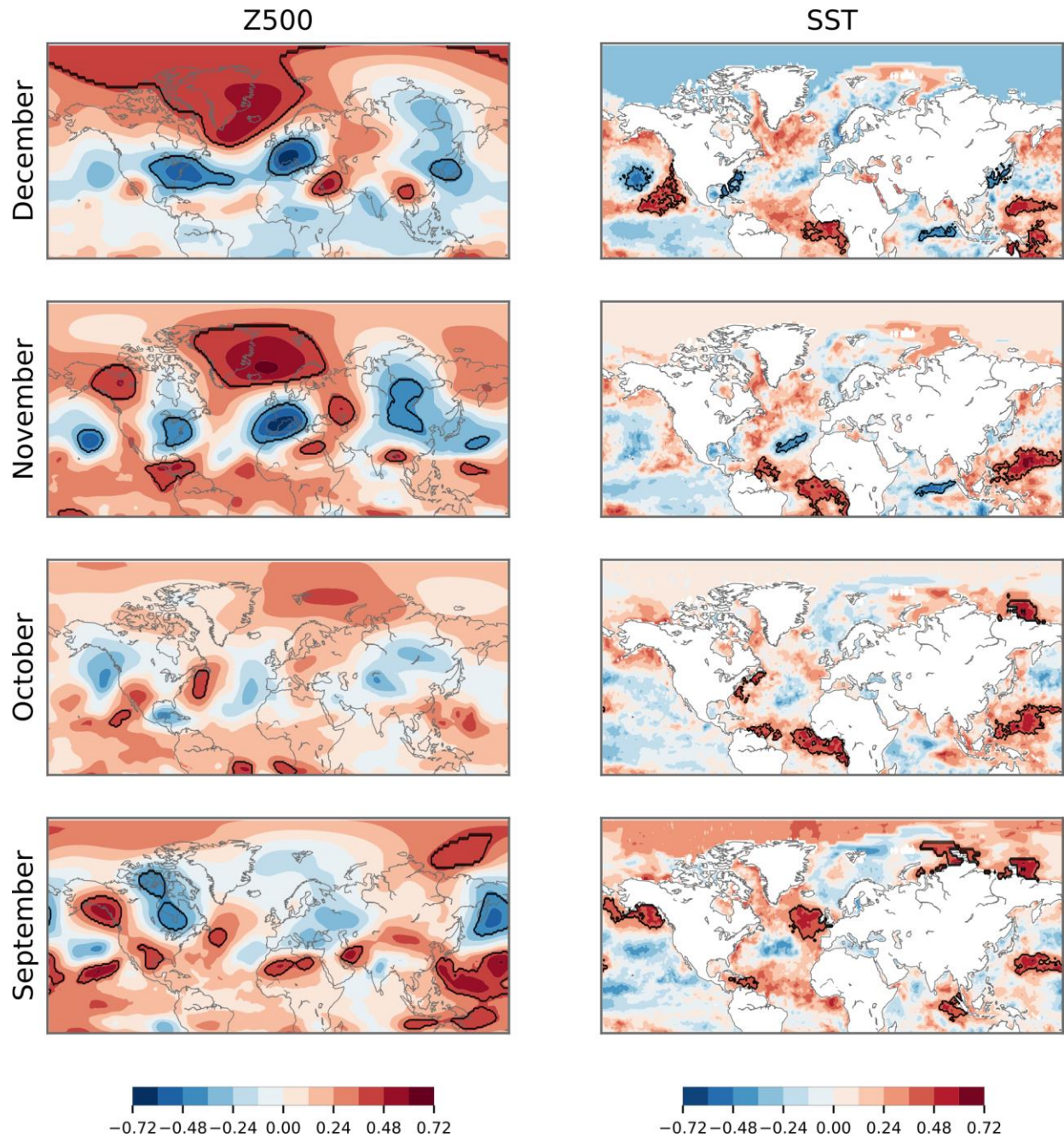150
151   **Step 3: Build the forecast model based on causal precursors**
152   In the last step we perform a multiple-linear regression between the anomaly time series of the
153   selected causal precursors and MWY anomalies to build the forecast model in the form
154    $\text{MWY}_{\text{forecast}} = \alpha + \sum_i^n \beta_i \cdot \text{CP}_i + \varepsilon_i$, where α is the intercept, β_i is the parameter of the i-th causal
155   precursor (CP_i) with error term ε_i and n is the total number of causal precursors.
156

157   **4 Results**

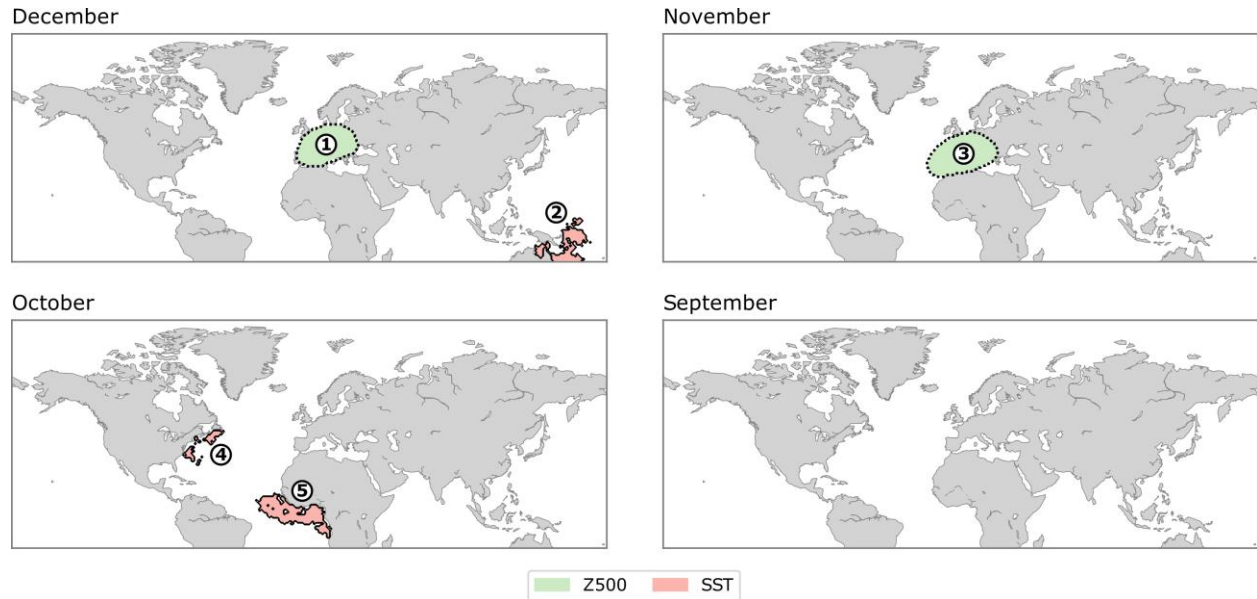158   **4.1 Extracting causal precursors from climate data**

159   In total 61 potential precursors are extracted (step 1) from the pairwise correlation analysis
160   between the gridded climate variables and MWY anomalies indicating both positive as well as
161   negative correlations (respective red and blue regions with contours in Fig. 1). Potential
162   precursors are found in each correlation map with spatial patterns of Z500 precursors showing
163   larger differences between time lags compared to SST as expected from higher variability in the

Fig. 1: Potential precursors derived from 500 hPa geopotential height anomaly fields (Z500, left) and sea surface temperature anomaly fields (SST, right). Pairwise correlations are calculated between wheat yield anomalies and the respective climate variable at each grid cell and time lag ranging from lag 4 (December) to lag 7 (September). Significantly correlated grid cells are then aggregated to homogeneous regions using cluster analysis (black contours).

atmosphere. Correlation maps are robust with similar regions found for different significance thresholds and subsamples of the studied time period (see details in Supporting Information (SI), Fig. S1).

173

Fig. 2: Causal precursors of Moroccan wheat yield anomalies. Five causal precursor regions
are extracted from geopotential height anomaly fields (Z500, green) and sea surface temperature
anomalies (SST, red) at different time lags. Contours indicate whether a precursor is positively
(solid line) or negatively (dotted line) correlated with yield anomalies.

178

Amongst all 61 potential precursors only five are found to be causally linked to WWY anomalies
following step 2 of the model building approach (Fig. 2). These causal precursors include a
region of negatively correlated Z500 anomalies over Central to Southwestern Europe in
November and December suggesting that Z500 anomalies in these months provide relevant,
independent information for MWY. Otherwise, the applied causal discovery algorithm should
have eliminated one of the two precursors during the conditional independence test. Consistently,
the correlation between both Z500 regions is only weak (Pearson correlation coefficient of
r=0.36, Fig. S2). A second causal precursor is found in December which refers to positively
correlated SST anomalies in the Coral Sea northwest of Australia. Two causal precursors emerge
in October and relate to positively correlated SST anomaly fields – one in the North Atlantic off
the East Cost of the USA and the other in the tropical Atlantic along the western African
coastline. In September no causal precursor for MWY is identified.

191

We test the robustness of the causal selection step by altering significance thresholds and
applying them to subsamples of the data and overall find consistent results (see detailed
discussion in SI, Fig. S3). Particularly, causal precursors 1-4 only show little sensitivity to the
chosen settings.

196

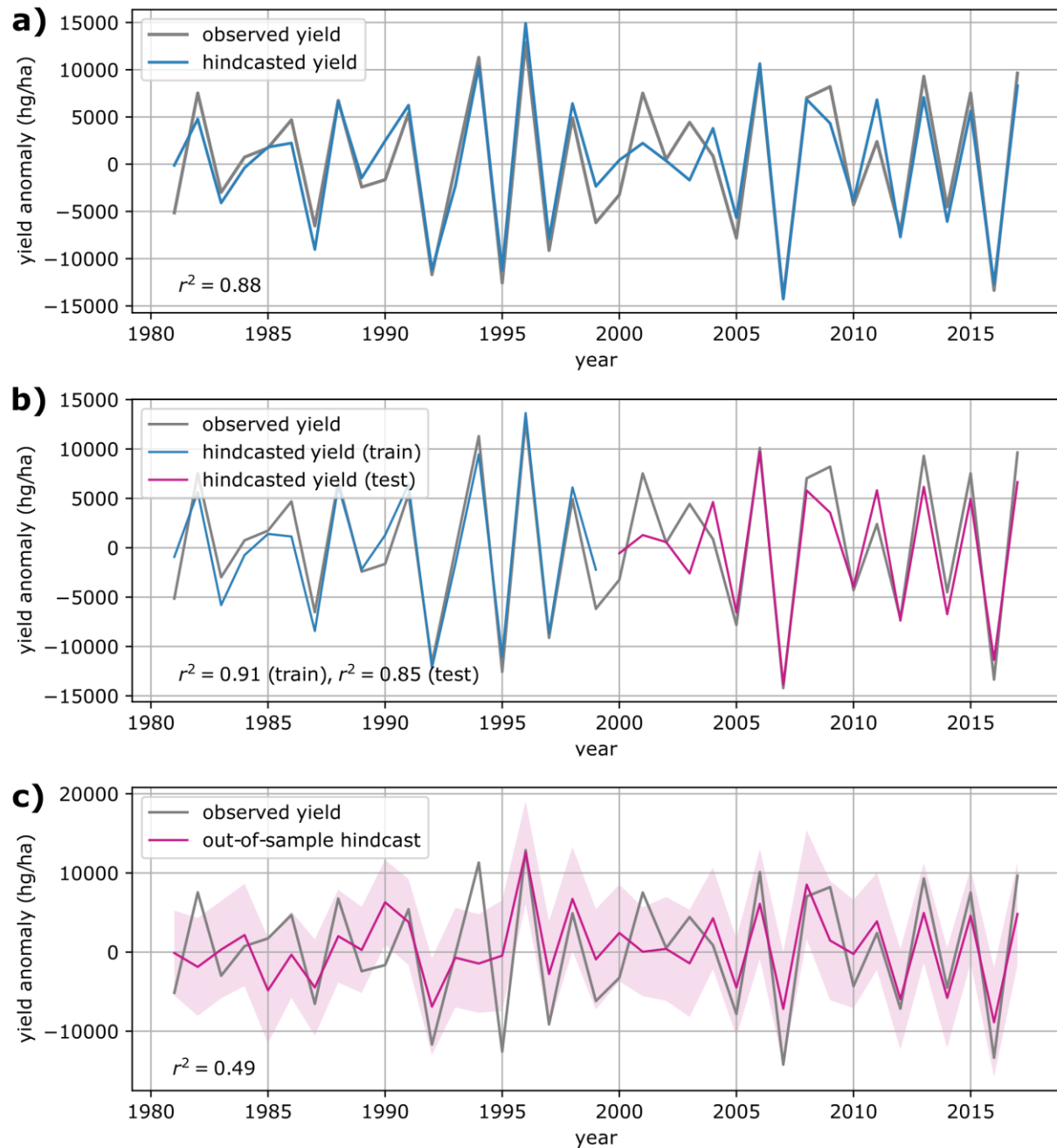197 **4.2 Validation of the Moroccan wheat yield hindcasts**

198 Hindcasted yield anomalies strongly correlate with observed anomalies, explaining 88% of the
199 observed yield variance over the full time period (Fig. 3a). Thereby, each causal precursor
200 contributes a similar individual share of 15-25% to the total explained variance (Fig. S4) as
201 computed from variance decomposition of the multiple-linear regression model (Grömping,
202 2007). Oscillating MWY variability over the last decade seems to be driven by similar variability
203 of the causal Z500 precursor regions in December and November (Fig. S5) which is in line with
204 an increased correlation strength over time between both precursors and MWY (Fig. S6). In
205 contrast, correlation strength between MWY and the causal SST precursor in the equatorial
206 Atlantic starts at a high level of around r=0.8 and then decreases to around r=0.4 in 2010. The
207 transition phase when the correlation of MWY with the Z500 precursors becomes stronger than
208 with the SST precursor corresponds to the time period where hindcasts diverge most from
209 observations (1999-2003) and may thus play a role for this discrepancy. Analyses of the hindcast
210 residuals confirm that the assumptions of a multiple-linear regression model are fulfilled; that is
211 that residuals are characterized by a mean value of zero, constant variance (homoscedasticity),
212 no significant auto-correlation and follow a normal distribution (Fig. S7).
213
214 The regression model is robust with respect to its regression parameters of the identified causal
215 precursors. To show this we divide the time series into two parts; regression parameters are
216 derived from the training period (19 years, 1981-1999) and then used to hindcast MWY
217 anomalies over the test period (18 years, 2000-2017). The explained variance over the training
218 period (91%) is high and similar to the explained variance over the test period (85%), indicating
219 that the regression model does not suffer from overfitting given the hypothetical case that all five
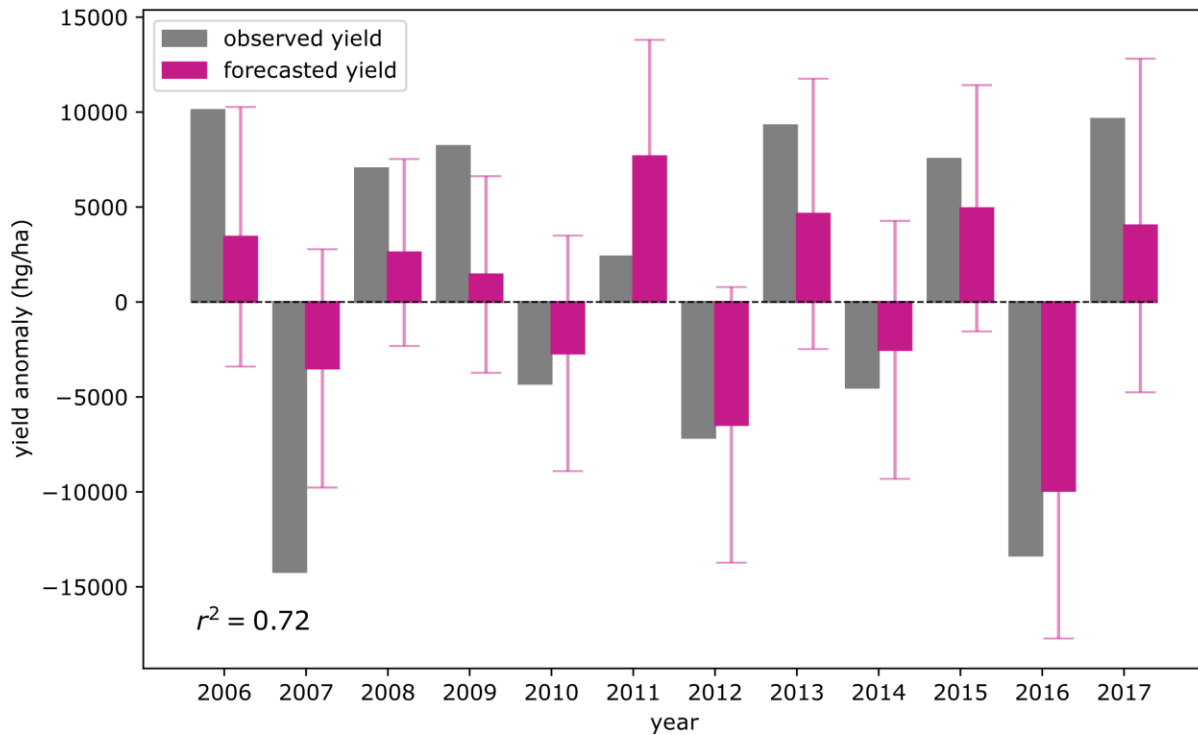220 causal precursors were known (Fig. 3b).
221
222 We next implement an out-of-sample cross validation to further validate the predictive skill of
223 our hindcast model in the case that causal precursors are not know a priori. For this, we
224 iteratively remove two consecutive years from the time series with the remaining years serving
225 as the training period and the left-out years as the test period. We choose to remove two
226 consecutive years instead of just one to account for the strong year-to-year autocorrelation of the
227 causal precursor time series (Fig. S8). The full hindcast model (step1-3) is then calculated using
228 data from the training period only to ensure that data against which the model skill is validated
229 does not enter any part of the model building process.
230
231 Hindcasted yield anomalies from this cross validation still explain 46% of the observed variance
232 over the full time period with observations mostly staying within the 95% prediction interval
233 (Fig. 3c). The drop in explained variance is due to the fact that not all five causal precursors are
234 detected in each training period which is primarily due to small changes in the identified
235 potential precursor sets. Repeating the cross-validation using prescribed potential precursors
236 from the full time period increases the explained variance to 76% (Fig. S9).

237
238 **Fig. 3 Hindcasts based on causal precursors.** (a) Hindcasted yields strongly correlate with
239 observed yields over the studied time period. (b) Observed and hindcasted yields over a train and
240 a test period with same causal precursors as in (a) and regression parameters calculated from the
241 train period only. (c) Leave-2-out cross validation with strict train-test splitting for all three
242 model building steps. Observed yields mostly stay within the 95% prediction interval.

243

Fig. 4: One-step-ahead forecast. The forecast model is iteratively computed from the 25-year period prior to the to-be-forecasted year. Vertical lines indicate the 95% prediction interval.

246

4.3 Forecasting wheat yields and comparison to other statistical methods

We next assess the potential of our approach to forecast interannual MWY changes and find it to produce accurate forecasts when operated in a one-step ahead mode. For this, we use climate and yield data from the 25-year period prior to the to-be-forecasted year to build the full forecast model, i.e. to define potential precursors, select causal precursors and derive the regression parameters. Regression parameters are then applied to causal precursor aomalies from the 26th year to produce the forecast. Afterwards the 25-year period is shifted by one year to re-build the complete model used to forecast the next year and so on. This way, possible long-term changes in teleconnections affecting MWY can in principle be captured. The forecast model accurately forecasts MWY anomalies showing the right direction of change in each year and explaining 72% of its variance between 2006 and 2017. Years before 2006 could not be tested because of a required reasonably long training period prior to the forecasted year. Observed yield anomalies are within the 95% prediction interval except for 2007 and 2016 where the observed decline in yield is significantly lower than forecasted and in 2009 where the observed yield anomaly is significantly higher.

264

265   To assess the added value of our forecast model we compare results to two simple forecast

266   models; one which assumes that the forecasted yield is equal to the average of historical yields

267   plus a linear trend and a second one which sets all forecasts to be the anomaly of the previous

268   year but inversed in sign (see details in SI, Fig. S10-S11). The latter model has no physical

269   meaning but is motivated by the characteristic time series of strongly alternating yield anomalies.

270   The average+trend model and the previous-year model show some skill in forecasting next

271   year's yield during 2006-2017 (r^2 = 0.71 and 0.58, respectively). However, predictive skill

272   drastically decreases in the out-of-sample cross validation with two years omitted in the training

273   phase (r^2 = 0.29 and 0.24, respectively), indicating that most of the skill in the forecast mode

274   comes from the strong year-to-year autocorrelation of MWY and causal precursor anomalies.

275   Our causal precursor based model outperforms both simple models by a factor of around two

276   with respect to explained variance.

277

5 Discussion and Conclusions

279   We have shown that Moroccan wheat yield anomalies which are strongly linked to winter

280   rainfall changes can be robustly predicted using five causal precursors extracted from

281   geopotential height anomalies at 500 hPa and sea surface temperatures. The physical

282   interpretation of the discovered links is discussed in the following.

283   A clear direct effect can be derived from the November and December geopotential height

284   anomalies over Europe indicated as causal precursors 1 and 3 (see Fig. 2). A high pressure

285   system over this region deflects extratropical storms to the north which bring moist air from the

286   Atlantic Ocean to the land (Hurrell, 1995). In turn, negative geopotential height anomalies would

287   favor more zonal storm tracks leading to more rainfall over Morocco (and thus higher yields)

288   consistent with the negative link we find between the precursors and wheat yields. The center

289   and spatial pattern of the two precursors resemble the southern region of pressure anomalies

290   characteristic for the North Atlantic Oscillation (NAO). Indeed, also the NAO counterpart of

291   positively correlated Z500 anomalies over Greenland/Iceland was identified in the correlation

292   maps (Fig. 1) but not found to add additional information for MWY. A strong link between NAO

293   and Moroccan precipitation has already been reported and used for predictions (El Hamly &

294   Sebbar, 1998; Jarlan et al., 2014; Knippertz et al., 2003). Here, this region is selected from our

295   data-driven method directly, confirming earlier findings.

296   The positive correlation between October SST anomalies at the East Coast of the USA (precursor

297   4, Fig. 2) and changes in wheat yields may arise via extratropical storm track activity. The causal

298   precursor region largely overlaps with a region of strong cyclogenesis of extratropical storms.

299   Cyclogenesis is largely determined by the surface layer and hence by sea surface temperatures

300   (Hoskins & Valdes, 1990). High temperature gradients in this region provide favorable

301   conditions for the creation of extratropical storms and thus increased storm track activity

302 associated with anomalously wet conditions over Europe and North Africa (Lehmann &
303 Coumou, 2015).

304 A more indirect effect can be assumed from both tropical sea surface temperature precursors on
305 Moroccan winter rainfall and thus wheat yields. There is an extensive body of literature on
306 tropical-extratropical interactions which explain how tropical thermal forcing impacts on
307 extratropical weather conditions through induced atmospheric responses (see e.g. Robertson &
308 Vitart, 2019 and references therein). The most important tropical-extratropical teleconnection at
309 the subseasonal to seasonal timescale emerges from the Madden-Julian Oscillation (MJO) (Stan
310 et al., 2017; Vitart, 2017). It has been shown that phase 6-7 of the MJO can enhance poleward
311 and vertical Rossby wave propagation leading to negative NAO-like conditions via a
312 stratospheric pathway (Lee et al., 2019) and thus positive precipitation anomalies over western
313 North Africa (Cassou, 2008; Lin et al., 2009). This link is in agreement with December precursor
314 2 in the West Pacific suggesting that it provides predictability for Moroccan wheat yields via its
315 remote influence on winter rainfall. The reported SST precursor 5 in October is consistent with a
316 documented tropical driver of Moroccan wheat yields. Warming of this region along the western
317 African coastline has been shown to enhance latitudinal moisture transport via changes in trade
318 winds which is important for autumn rainfall in Morocco and thus for the early phase of wheat
319 development (Knippertz et al., 2003).
320
321 The reported set of causal precursors is robust over the studied time period. However, for some
322 shorter time intervals only a subsample of the set is found to be significant. Assessing the origin
323 of these differences using data from climate models could give valuable insights into whether
324 this is a statistical artefact or due to actual changes in physical teleconnections. Moreover, albeit
325 all five causal precursors were found to be similarly important to forecast Moroccan wheat
326 yields, each of them may be relevant for different phases of rainfall during the rainy season or
327 rainfall at different locations. For example, it has been suggested that pressure anomalies
328 consistent with precursor 1 are important for early wheat growth (Jarlan et al., 2014) whereas
329 tropical Pacific SSTs corresponding to precursor 2 are relevant for late-season precipitation (El
330 Hamly & Sebbar, 1998). This should be assessed in subsequent research by linking climate
331 drivers to spatially resolved rainfall over Morocco using the causal discovery algorithm
332 presented in this. Finally, further insights can be gained by analyzing how teleconnections
333 operating on longer timescales might affect the precursors identified in this study. For example,
334 Lee et al. (2019) showed that the El Niño Southern Oscillation (ENSO) influences the above
335 mentioned MJO-NAO link through modulation of the seasonal mean background state.
336
337 Recent research showed the great potential of teleconnections as a source of predictability on
338 subseasonal to seasonal timescales, relevant for a multitude of applications (Dobrynin et al.,
339 2018; Merryfield et al., 2020; White et al., 2017). Here we showed that climatic information can
340 be used to forecast Moroccan wheat yields four months before harvest through its direct link to
341 prevailing rainfall conditions. Such long lead times could significantly improve strategic

342 adaptation measures from the state to farm level including early wheat import planning, the
343 application of plant protection materials and fertilizers, and provide humanitarian actors with
344 timely information for early action. The presented method can easily be transferred to other
345 indicators and regions. Yet, we emphasize that expert knowledge, e.g. about appropriate climate
346 precursors, and a careful interpretation of the results is crucial to extract meaningful results.

356 **References**

357 Balaghi, R., Tychon, B., Eerens, H., & Jlibene, M. (2008). Empirical regression models using NDVI,
358   rainfall and temperature data for the early prediction of wheat grain yields in Morocco.
359   *International Journal of Applied Earth Observation and Geoinformation*, *10*(4), 438–452.
360   https://doi.org/10.1016/j.jag.2006.12.001

361 Berdai, H., Karrou, M., Chati, M. T., Boutfirass, M., & Bekaou, A. (2011). Irrigation water
362   management in Morocco: a review. *In "Improving Water and Land Productivities in Rainfed*
363   *Systems, Community-Based Optimization of the Management of Scarce Water Resources in*
364   *Agriculture in CWANA. Report No. 8.*

365 Bernardi, M. (2016). Crop Yield Forecasting in Morocco. *Food and Agriculture Organization of*
366   *the United Nations*, (February).

367 Born, K., Fink, A. H., & Paeth, H. (2008). Dry and wet periods in the northwestern Maghreb for
368   present day and future climate conditions. *Meteorologische Zeitschrift*, *17*(5), 533–551.
369   https://doi.org/10.1127/0941-2948/2008/0313

370 Bregaglio, S., Frasso, N., Pagani, V., Stella, T., Francone, C., Cappelli, G., et al. (2014). New multi-
371   model approach gives good estimations of wheat yield under semi-arid climate in
372   Morocco. *Agronomy for Sustainable Development*, *35*(1), 157–167.
373   https://doi.org/10.1007/s13593-014-0225-6

374 Di Capua, G., Kretschmer, M., Runge, J., Alessandri, A., Donner, R. V., van den Hurk, B., et al.
375   (2019). Long-Lead Statistical Forecasts of the Indian Summer Monsoon Rainfall Based on

376   Causal Precursors. *Weather and Forecasting*, *34*(5), 1377–1394.
377   https://doi.org/10.1175/WAF-D-19-0002.1

378 Cassou, C. (2008). Intraseasonal interaction between the Madden-Julian Oscillation and the
379   North Atlantic Oscillation. *Nature*, *455*(7212), 523–527.
380   https://doi.org/10.1038/nature07286

381 Dobrynin, M., Domeisen, D. I. V., Müller, W. A., Bell, L., Brune, S., Bunzel, F., et al. (2018).
382   Improved Teleconnection-Based Dynamical Seasonal Predictions of Boreal Winter.
383   *Geophysical Research Letters*, *45*(8), 3605–3614. https://doi.org/10.1002/2018GL077209

384 Ester, M., Kriegel, H. P., Sander, J., & Xu, X. (1996). A Density-Based Algorithm for Discovering
385   Clusters in Large Spatial Databases with Noise. In: Proceedings of the 2nd International
386   Conference on Knowledge Discovery and Data Mining, Portland, OR, AAAI Press. Elsevier.
387   Elsevier.

388 FAOSTAT. (2017). Moroccan Wheat Yield Data. Retrieved from
389   http://www.fao.org/faostat/en/#data

390 Filahi, S., Tramblay, Y., Mouhir, L., & Diaconescu, E. P. (2017). Projected changes in temperature
391   and precipitation indices in Morocco from high-resolution regional climate models.
392   *International Journal of Climatology*, *37*(14), 4846–4863. https://doi.org/10.1002/joc.5127

393 Grömping, U. (2007). Estimators of relative importance in linear regression based on variance
394   decomposition. *American Statistician*, *61*(2), 139–147.
395   https://doi.org/10.1198/000313007X188252

396 El Hamly, M., & Sebbar, R. (1998). Towards the seasonal prediction of Moroccan precipitation
397   and its implications for water resources management. *Proceeding of the Abidjan '9*
398   *Conference*, *252*, 476.

399 Hersbach, H., Bell, B., Berrisford, P., Horányi, A., Sabater, J. M., Nicolas, J., et al. (2019). Global
400   reanalysis: goodbye ERA-Interim, hello ERA5. *ECMWF Newsletter*, (159), 17–24.
401   https://doi.org/10.21957/vf291hehd7

402 Hoskins, B., & Valdes, P. (1990). On the existence of storm-tracks. *Journal of the Atmospheric*
403   *Sciences*, *47*(15), 1854–1864. https://doi.org/10.1175/ 1520-
404   0469(1990)047,1854:OTEOST.2.0.CO;2

405 Hurrell, J. W. (1995). Decadal trends in the north atlantic oscillation: regional temperatures and
406   precipitation. *Science (New York, N.Y.)*, *269*(5224), 676–679.
407   https://doi.org/10.1126/science.269.5224.676

408 Jarlan, L., Abaoui, J., Duchemin, B., Ouldbba, A., Tourre, Y. M., Khabba, S., et al. (2014). Linkages
409   between common wheat yields and climate in Morocco (1982-2008). *International Journal*
410   *of Biometeorology*, *58*(7), 1489–1502. https://doi.org/10.1007/s00484-013-0753-9

411   Knippertz, P., Christoph, M., & Speth, P. (2003). Long-term precipitation variability in Morocco
412   and the link to the large-scale circulation in recent and future climates. *Meteorology and*
413   *Atmospheric Physics*, *83*(1–2), 67–88. https://doi.org/10.1007/s00703-002-0561-y

414   Kretschmer, M., Coumou, D., Donges, J. F., & Runge, J. (2016). Using Causal Effect Networks to
415   Analyze Different Arctic Drivers of Midlatitude Winter Circulation. *Journal of Climate*,
416   *29*(11), 4069–4081. https://doi.org/10.1175/JCLI-D-15-0654.1

417   Kretschmer, M., Runge, J., & Coumou, D. (2017). Early prediction of extreme stratospheric polar
418   vortex states based on causal precursors. *Geophysical Research Letters*, 1–9.
419   https://doi.org/10.1002/2017GL074696

420   Lee, R. W., Woolnough, S. J., Charlton-Perez, A. J., & Vitart, F. (2019). ENSO Modulation of MJO
421   Teleconnections to the North Atlantic and Europe. *Geophysical Research Letters*, *n/a*(n/a).
422   https://doi.org/10.1029/2019GL084683

423   Lehmann, J., & Coumou, D. (2015). The influence of mid-latitude storm tracks on hot, cold, dry
424   and wet extremes. *Scientific Reports*, *5*(1), 17491. https://doi.org/10.1038/srep17491

425   Lin, H., Brunet, G., & Derome, J. (2009). An Observed Connection between the North Atlantic
426   Oscillation and the Madden–Julian Oscillation. *Journal of Climate*, *22*(2), 364–380.
427   https://doi.org/10.1175/2008JCLI2515.1

428   Merryfield, W. J., Baehr, J., Batté, L., Becker, E. J., Butler, A. H., Coelho, C. A. S., et al. (2020).
429   Current and emerging developments in subseasonal to decadal prediction. *Bulletin of the*
430   *American Meteorological Society*, BAMS-D-19-0037.1. https://doi.org/10.1175/BAMS-D-
431   19-0037.1

432   Robertson, A. W., & Vitart, F. (2019). *Subseasonal to Seasonal Prediction: The Gap Between*
433   *Weather and Climate Forecasting*. Elsevier.

434   Rodríguez-Fonseca, B., Polo, I., Serrano, E., & Castro, M. (2006). Evaluation of the North Atlantic
435   SST forcing on the European and Northern African winter climate. *International Journal of*
436   *Climatology*, *26*(2), 179–191. https://doi.org/10.1002/joc.1234

437   Runge, J. (2018). Causal network reconstruction from time series: From theoretical assumptions
438   to practical estimation. *Chaos: An Interdisciplinary Journal of Nonlinear Science*, *28*(7),
439   075310. https://doi.org/10.1063/1.5025050

440   Runge, Jakob, Bathiany, S., Bollt, E., Camps-Valls, G., Coumou, D., Deyle, E., et al. (2019).
441   Inferring causation from time series in Earth system sciences. *Nature Communications*,
442   *10*(1), 2553. https://doi.org/10.1038/s41467-019-10105-3

443   Schlueter, A., Fink, A. H., Knippertz, P., & Vogel, P. (2019). A Systematic comparison of tropical
444   waves over northern Africa. Part I: Influence on rainfall. *Journal of Climate*, *32*(5), 1501–
445   1523. https://doi.org/10.1175/JCLI-D-18-0173.1

446   Schubert, E., Sander, J., Ester, M., Kriegel, H. P., & Xu, X. (2017). DBSCAN Revisited, Revisited.
447   *ACM Transactions on Database Systems*, *42*(3), 1–21. https://doi.org/10.1145/3068335

448   Shaman, J., & Tziperman, E. (2011). An Atmospheric Teleconnection Linking ENSO and
449   Southwestern European Precipitation. *Journal of Climate*, *24*(1), 124–139.
450   https://doi.org/10.1175/2010JCLI3590.1

451   Stan, C., Straus, D. M., Frederiksen, J. S., Lin, H., Maloney, E. D., & Schumacher, C. (2017).
452   Review of Tropical-Extratropical Teleconnections on Intraseasonal Time Scales. *Reviews of*
453   *Geophysics*, *55*(4), 902–937. https://doi.org/10.1002/2016RG000538

454   Tuel, A., & Eltahir, E. A. B. (2018). Seasonal Precipitation Forecast Over Morocco. *Water*
455   *Resources Research*, *54*(11), 9118–9130. https://doi.org/10.1029/2018WR022984

456   Vitart, F. (2017). Madden—Julian Oscillation prediction and teleconnections in the S2S
457   database. *Quarterly Journal of the Royal Meteorological Society*, *143*(706), 2210–2220.
458   https://doi.org/10.1002/qj.3079

459   White, C. J., Carlsen, H., Robertson, A. W., Klein, R. J. T., Lazo, J. K., Kumar, A., et al. (2017).
460   Potential applications of subseasonal-to-seasonal (S2S) predictions. *Meteorological*
461   *Applications*, *24*(3), 315–325. https://doi.org/10.1002/met.1654

462   De Wit, A., Hoek, S., Ballaghib, R., El Hairechc, T., & Dong, Q. (2013). Building an operational
463   system for crop monitoring and yield forecasting in Morocco. *2013 2nd International*
464   *Conference on Agro-Geoinformatics: Information for Sustainable Agriculture, Agro-*
465   *Geoinformatics 2013*, 466–469. https://doi.org/10.1109/Argo-
466   Geoinformatics.2013.6621964

467